ACS APPLIED MATERIALS & INTERFACES

Research Article

www.acsami.org

Insights into the Morphological Instability of Bulk Heterojunction PTB7-Th/PCBM Solar Cells upon High-Temperature Aging

Yen-Ju Hsieh,[†,‡] Yu-Ching Huang,[§] Wei-Shin Liu,[†,‡] Yu-An Su,[†,⊗] Cheng-Si Tsao,*[,§,#] Syang-Peng Rwei,[⊥] and Leeyih Wang*[,†,‡]

[†]Centre for Condensed Matter Sciences, National Taiwan University, Taipei 10617, Taiwan

[‡]Institute of Polymer Science and Engineering, National Taiwan University, Taipei 10617, Taiwan

[§]Institute of Nuclear Energy Research, Longtan, Taoyuan 32546, Taiwan

[⊥]Institute of Organic and Polymeric Materials, National Taipei University of Technology, Taipei 10608, Taiwan

[#]Department of Materials Science and Engineering, National Taiwan University, Taipei 10617, Taiwan

[⊗]Materials Science Division, Argonne National Laboratory, 9700 Cass Avenue, Lemont, Illinois 60439, United States

Supporting Information

ABSTRACT: The impact of the morphological stability of the donor/acceptor mixture under thermal stress on the photovoltaic properties of bulk heterojunction (BHJ) solar cells based on the poly[4,8-bis(5-(2-ethylhexyl)thiophen-2-yl)benzo[1,2-*b*;4,5-*b*′]-dithiophene-2,6-diyl-*alt*-(4-(2-ethylhexyl)-3-fluorothieno[3,4-*b*]-thiophene)-2-carboxylate-2,6-diyl]/phenyl-C_{61}-butyric acid methyl ester (PTB7-Th/$PC_{61}BM$) blend is extensively investigated. Both optical microscopy and transmission electron microscopy micrographs show that long-term high-temperature aging stimulates the formation of microscale clusters, the size of which, however, is about 1 order of magnitude smaller than those observed in thermally annealed poly(3-hexylthiophene)/$PC_{61}BM$ composite film. The multilength-scale evolution of the morphology of PTB7-Th/$PC_{61}BM$ film from the scattering profiles of grazing incidence small-angle and wide-angle X-ray scattering indicates the $PC_{61}BM$ molecules spatially confine the self-organization of polymer chains into large domains during cast drying and upon thermal activation. Moreover, some $PC_{61}BM$ molecules accumulate into ∼30−40 nm clusters, the number of which increases with heating time. Therefore, the hole mobility in the active layer decays much more rapidly than the electron mobility, leading to unbalanced charge transport and degraded cell performance. Importantly, the three-component blend that is formed by replacing a small amount of $PC_{61}BM$ in the active layer with the bis-adduct of $PC_{61}BM$ (bis-$PC_{61}BM$) exhibits robust morphology against thermal stress. Accordingly, the PTB7-Th/$PC_{61}BM$:bis-$PC_{61}BM$ (8 wt %) device has an extremely stable power conversion efficiency.

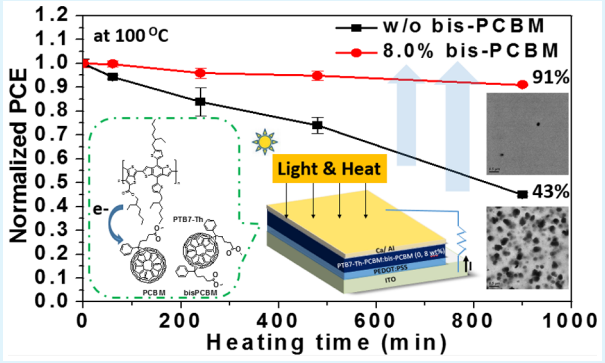

KEYWORDS: *morphology evolution, polymer solar cells, bulk heterojunction, thermal stability, X-ray scattering*

INTRODUCTION

Polymer solar cells (PSCs), which comprise a semiconducting polymer as an electron donor and a fullerene derivative as an electron acceptor, have attracted considerable attention in recent decades because of their great potential in providing mobile renewable energy at low cost.[1−3] Recent rapid progress in the development of low-bandgap (LBG) polymers with enhanced light-harvesting ability, adequate energy levels, and favorable hole mobility resulted in the increased power conversion efficiency (PCE) of single-junction PSCs to >10%.[4] Among abundant LBG polymers, the polythieno[3,4-*b*]-thiophene-*co*-benzodithiophene family that was developed by Yu et al. has become one of the most extensively studied donor materials owing to its unique properties.[5] When a mixture of dichlorobenzene and 1,8-diiodoctane (DIO) is used as the processing solvent for a bulk heterojunction (BHJ) solar cell that was based on the blend of poly({4,8-bis[(2-ethylhexyl)oxy]benzo[1,2-*b*:4,5-*b*′]dithiophene-2,6-diyl}{3-fluoro-2-[(2-ethylhexyl)carbonyl]thieno[3,4-*b*]thiophenediyl}) (PTB7) and phenyl-C_{71}-butyric acid methyl ester ($PC_{71}BM$), an optimal morphology with reduced domain sizes and improved charge collection was attained, increasing the PCE of the cell to 7.4%.[6] Adopting an inverted device structure to this blend system and using poly[(9,9-bis(3′-(*N*,*N*-dimethylamino)propyl)-2,7-fluorene)-*alt*-2,7-(9,9-dioctylfluorene)] (PFN) as the surface modifier of the ITO cathode

Received: January 25, 2017
Accepted: April 11, 2017
Published: April 11, 2017

DOI: 10.1021/acsami.7b01296
ACS Appl. Mater. Interfaces 2017, 9, 14808−14816

successfully raised the PCE to 9.2%.[7] To improve the coplanarity of the backbone and to red-shift the absorption spectrum, two 2-ethylhexyl-thienyl groups were incorporated into the benzodithiophene unit in PTB7 to generate poly[4,8-bis(5-(2-ethylhexyl)thiophen-2-yl)benzo[1,2-*b*;4,5-*b*′]-dithiophene-2,6-diyl-*alt*-(4-(2-ethylhexyl)-3-fluorothieno[3,4-*b*]thiophene)-2-carboxylate-2,6-diyl] (PTB7-Th). The cell with the structure ITO/ZnO-C_{60}/PTB7-Th:$PC_{71}BM$/MoO_3/Ag exhibited a promising PCE of 9.35%.[8] Subsequently, Chen et al. increased the PCE to 10.32% by simultaneously doping the ZnO cathode with indium and a bisphenol-containing fullerene derivative.[9]

Both cell performance and operational lifetime are equally important to the commercialization of solar cells. It is well established that the morphology of donor/acceptor blends critically affects the photovoltaic processes of BHJ PSCs, including exciton dissociation, carrier transport, charge recombination, and collection.[10−14] Therefore, the optimization of morphology has become essential to maximizing the PCE of such devices.[15−19] Under the practical operational conditions, these solar cells are markedly heated by long-term illumination of sunlight, and the actual operating temperature for solar panels can be as high as 50−70 °C, even reaching 100 °C at some areas.[20] However, the phase domains within the blends of the polymer donor and fullerene acceptor are frequently sensitive to high-temperature aging. For instance, storing the blend film of poly(3-hexylthiophene) (P3HT) and $PC_{61}BM$ in a 150 °C oven for 15 h induces the formation of numerous micrometer-sized clusters, reducing the PCE by around 80%.[21] In recent years, several effective approaches have been developed to solve this problem. One successful method is the use of a polymer donor with less crystallinity or a high glass transition temperature and,[22,23] therefore, a weaker ability to undergo ordered packing through thermal motion. The incorporation of a compatibilizer,[24] a block copolymer,[25] or a C_{60}-based phase separation inhibitor is also effective in preventing macroscale phase separation.[21] Another common scheme involves the use of cross-linkable,[26] amorphous,[27] multisubstituted or conjugated moiety-bearing fullerene derivatives as the acceptor.[28−31] In addition, a sturdy morphology can be achieved by forming hydrogen bonds between fullerene molecules and polymer chains in the active layer.[32]

The self-organization of LBG polymers that have a relatively complex molecular structure and a backbone which consists of electron-rich and electron-deficient units is considered to differ considerably from that of P3HT homopolymer. Hence, the phase segregation of the mixed solution of such a polymer and a fullerene acceptor is reasonably assumed to differ from that of the P3HT/$PC_{61}BM$ system. It is reported that the hierarchical BHJ morphology of phase-separated PTB7-based polymer:$PC_{61}BM$ films is formed by polymer crystallization and $PC_{61}BM$ clustering.[5,33−36] However, the morphological stability and the thermal evolution of the multilength-scale morphology of the active layer based on LBG polymers and fullerene acceptors have rarely been investigated. The grazing incidence small-angle and wide-angle X-ray scattering (GISAXS and GIWAXS, respectively) techniques have been shown to be effective tools to investigate the hierarchical BHJ structure of PSCs.[11,37] This work first examined the effect of the thermal stability of phase domains in the PTB7-Th/$PC_{61}BM$ blend on the photovoltaic performance of the corresponding BHJ solar cells. An extensive exploration of the microscale to nanoscale evolution of morphology in various heating stages was then carried out using optical microscopy (OM), transmission electron microscopy (TEM), and synchrotron simultaneous GISAXS/GIWAXS techniques. Furthermore, we demonstrated that applying the bis-adduct of $PC_{61}BM$ (bis-$PC_{61}BM$) as the additive of the fullerene acceptor effectively stabilized the film morphology of PTB7-Th/$PC_{61}BM$ against long-term annealing at 100 °C.[20] The mutual influences among the structural evolutions of polymer crystallization, nanoscale $PC_{61}BM$ clustering, and mesoscale aggregation in the multilength-scale structure during heating period are revealed herein and correlated to the performance. The underlying mechanism for the formation of this robust three-component polymer/fullerene blend is then proposed.

RESULTS AND DISCUSSION

The effect of the morphological stability of the PTB7-Th/$PC_{61}BM$ active layer on the performance of BHJ solar cells was examined by aging such a composite layer at 100 °C for various periods in a glovebox, which provided an environment of low moisture and low oxygen concentration to prevent interference by chemical oxidation, before the top metal electrode is deposited to complete the fabrication of the device. Figure 1

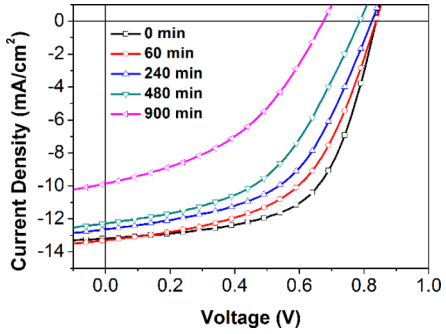

Figure 1. *J*−*V* curves of PTB7-Th/$PC_{61}BM$ devices under AM 1.5 G illumination at 100 mW/cm² with long-term thermal annealing at 100 °C.

plots the *J*−*V* curves of these cells, which were measured under AM 1.5 G illumination. As shown in Table 1, all photovoltaic

Table 1. Photovoltaic Characteristics of the PSCs Based on PTB7-Th:$PC_{61}BM$ (1:1.5, w/w) after Isothermal Annealing at 100 °C for Various Periods

annealing time (min)	V_{oc} (mV)	J_{sc} (mA/cm²)	FF (%)	PCE (%)
0	838 ± 10	13.29 ± 0.25	59.7 ± 2.5	6.65 ± 0.22
60	833 ± 6	13.26 ± 0.03	53.5 ± 0.2	5.92 ± 0.05
240	813 ± 38	12.66 ± 0.04	51.0 ± 1.3	5.26 ± 0.37
480	788 ± 21	12.22 ± 0.04	48.2 ± 1.0	4.64 ± 0.21
900	678 ± 10	9.89 ± 0.06	42.2 ± 0.2	2.83 ± 0.05

parameters, including open-circuit voltage (V_{oc}), short-circuit current density (J_{sc}), and fill factor (FF), monotonically degrade as the aging time increases, reducing the PCE to <3% after 15 h of isothermal heating at 100 °C. This observation clearly reveals that the optimal morphology of the PTB7-Th/$PC_{61}BM$ blend is highly sensitive to thermal stress.

We previously demonstrated that bis-$PC_{61}BM$ can be utilized as a phase-separation inhibitor to stabilize the morphology of P3HT/$PC_{61}BM$ blends in a high-temperature environment

DOI: 10.1021/acsami.7b01296
ACS Appl. Mater. Interfaces 2017, 9, 14808−14816

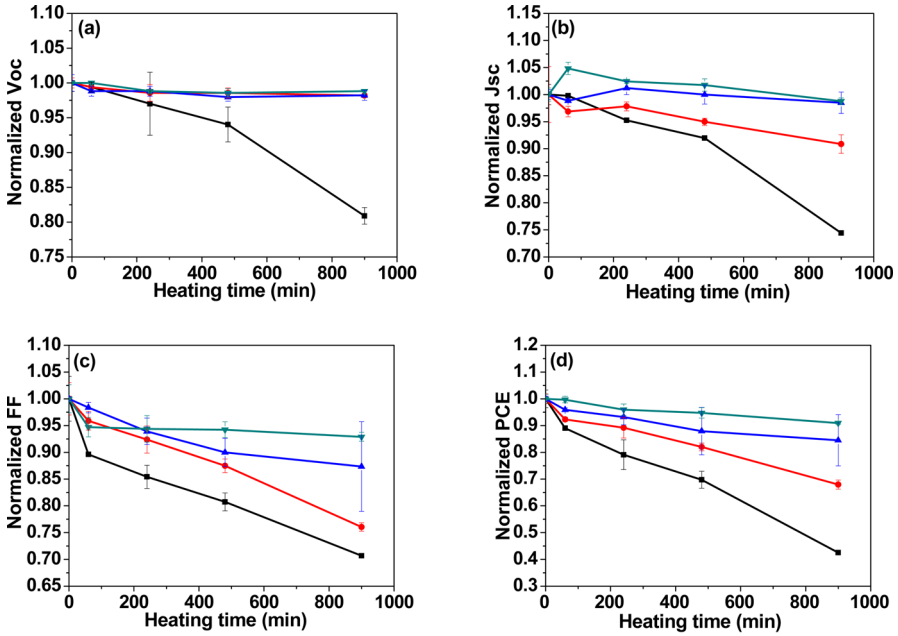

Figure 2. Influence of thermal aging at 100 °C on the (a) V_{oc}, (b) J_{sc}, (c) FF, and (d) PCE of the PTB7-Th/$PC_{61}BM$:bis-$PC_{61}BM$ solar cells with bis-$PC_{61}BM$ contents of 0 (black boxes), 2 (red circles), 4 (blue triangles), and 8 (green triangles) wt %.

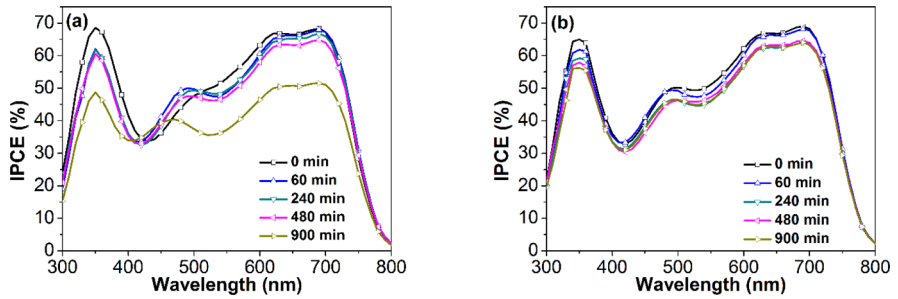

Figure 3. IPCE spectra of the solar devices based on (a) PTB7-Th/$PC_{61}BM$ and (b) PTB7-Th/$PC_{61}BM$:bis-$PC_{61}BM$ (8 wt %) after isothermal annealing at 100 °C for various periods.

owing to its amorphous nature and two bulky substituents, which prevent close contact between fullerene cages.[21] This approach has the advantage of the continuous use of a benchmark acceptor, $PC_{61}BM$, and the similar solubility and chemical compatibility of both fullerene derivatives. Herein, some of the $PC_{61}BM$ in the PTB7-Th/$PC_{61}BM$ blend was replaced with bis-$PC_{61}BM$ to generate a three-component photoactive layer. Figure S1 plots the $J-V$ curves of the PTB7-Th/$PC_{61}BM$ with and without bis-$PC_{61}BM$, and Table S1 in the Supporting Information presents the extracted photovoltaic parameters. Interestingly, bis-$PC_{61}BM$ in the active layer has a minor effect on V_{oc} and FF, although bis-$PC_{61}BM$ has a lower electron mobility and higher-lying HOMO than $PC_{61}BM$. An acceptor mixture of 98% $PC_{61}BM$ with 2% bis-$PC_{61}BM$ slightly improves the photocurrent and fill factor, yielding a V_{oc} of 835 mV, a J_{sc} of 13.34 mA/cm^2, an FF of 63.1%, and, therefore, a promising PCE of 7.02%. This is probably because the bulky bis-$PC_{61}BM$ molecules hinder the growth of numbers of pristine $PC_{61}BM$ aggregates during the spin-drying procedure, consequently increasing the interfacial area between the polymer donor and fullerene acceptor and promoting the formation of percolated $PC_{61}BM$/bis-$PC_{61}BM$ pathways to the cathode.[21] However, the cell performance slowly decreases as the bis-$PC_{61}BM$ loading is greater than 2 wt % because of the low carrier-mobility nature of bis-$PC_{61}BM$.

The long-term thermal stability of bulk heterojunction PTB7-Th/$PC_{61}BM$, PTB7-Th/$PC_{61}BM$:bis-$PC_{61}BM$ (2 wt %), PTB7-Th/$PC_{61}BM$:bis-$PC_{61}BM$ (4 wt %), and PTB7-Th/$PC_{61}BM$:bis- $PC_{61}BM$ (8 wt %) solar cells was investigated using the procedure described above to determine the durability of the PTB7-Th/$PC_{61}BM$ device. Figure 2 plots the dependences of major photovoltaic parameters of these cells on thermal aging time, and Table S2 presents the relevant numerical values. Evidently, the incorporation of a tiny amount of bis-$PC_{61}BM$ into the active layer successfully stabilizes both V_{oc} and J_{sc} against long-time–high-temperature stress, as displayed in Figure 2a,b. The increment of the mass loading of bis-$PC_{61}BM$ from 2 to 8% further slows the decay of FF (Figure 2c). Consequently, the thermally induced degradation of PCE is substantially reduced from 57% for the device without bis-$PC_{61}BM$ to <32% for that with bis-$PC_{61}BM$. Especially, the cell with 8 wt % bis-$PC_{61}BM$ exhibits a very steady PCE, retaining ~91% of the initial PCE even at thermal stress at 100 °C for 15 h (Figure 2d).

Panels a and b of Figure 3 show the incident photon-to-current conversion efficiency (IPCE) spectra of the PTB7-Th/$PC_{61}BM$ and PTB7-Th/$PC_{61}BM$:bis-$PC_{61}BM$ (8 wt %) solar

DOI: 10.1021/acsami.7b01296
ACS Appl. Mater. Interfaces 2017, 9, 14808–14816

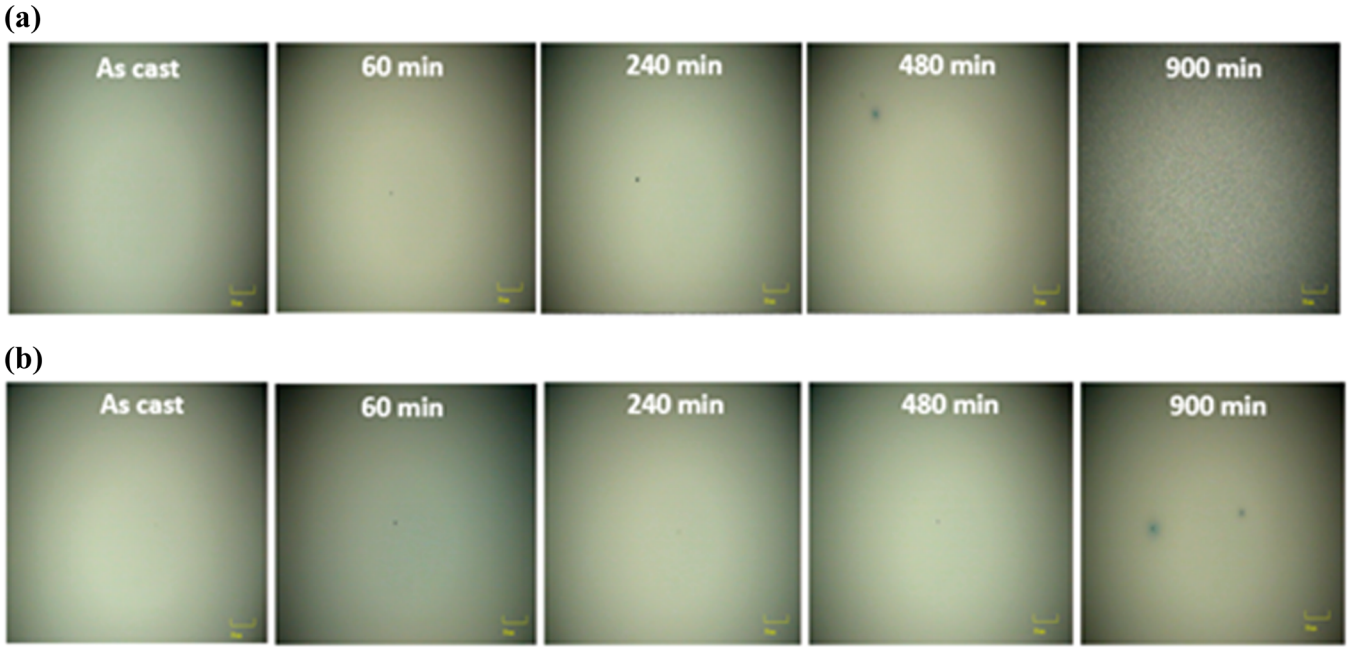

Figure 4. OM images of (a) PTB7-Th/$PC_{61}BM$ and (b) PTb7-Th/$PC_{61}BM$:bis-$PC_{61}BM$ (8 wt %) composite films after thermal aging at 100 °C for various periods.

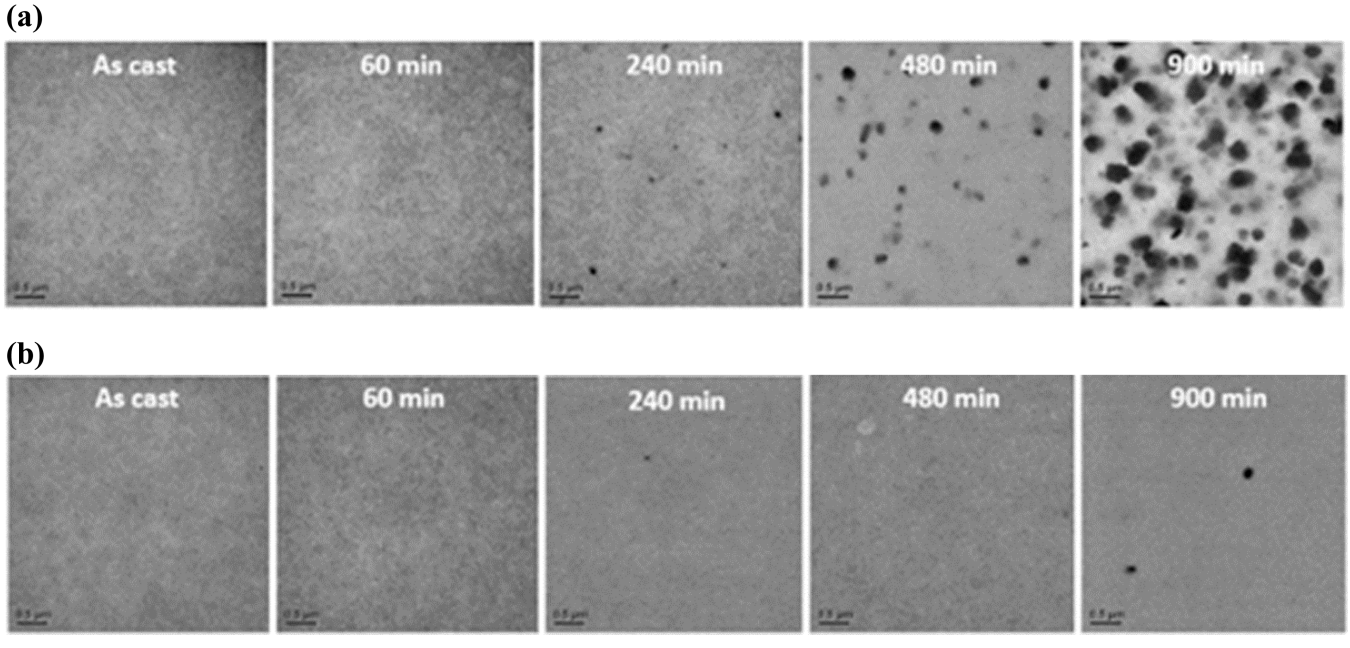

Figure 5. TEM images of (a) PTB7-Th/$PC_{61}BM$ and (b) PTB7-Th/$PC_{61}BM$:bis-$PC_{61}BM$ (8 wt %) composite films after thermal aging at 100 °C for various periods.

cells, respectively, after various heating times. All spectra are basically similar in shape, suggesting that the change in morphology is the main cause of the reduction of photocurrent. The IPCE of the PTB7-Th/$PC_{61}BM$ device drops continuously with increasing aging time. This result agrees closely with the trend of J_{sc} in Table S2 in terms of decreasing tendency and reduced ratio in numerical values. However, the PTB7-Th/$PC_{61}BM$:bis-$PC_{61}BM$ (8 wt %) device maintains steady IPCE values over the entire range of wavelengths during long-term thermal aging, as expected.

OM was employed to examine preliminarily the evolution of the morphology of thermally aged spin-coated films of PTB7-Th/$PC_{61}BM$ and PTB7-Th/$PC_{61}BM$:bis-$PC_{61}BM$ (8 wt %) composites. The images in Figure 4 reveal that both as-cast films have smooth and featureless surfaces. However, 15 h of aging at 100 °C induces the appearance of countless black dots in Figure 4a, revealing the thermal instability of phase domains in the PTB7-Th/$PC_{61}BM$ film. Conversely, such thermal stress has no detectable impact on the PTB7-Th/$PC_{61}BM$:bis-$PC_{61}BM$ (8 wt %) film, confirming that bis-$PC_{61}BM$ can be used as an effective morphology stabilizer for the PTB7-Th/$PC_{61}BM$ system as well (Figure 4b).

Then, TEM was applied to capture images of the two films at nanoscale resolution. The TEM pictures in Figure 5a show that

DOI: 10.1021/acsami.7b01296
ACS Appl. Mater. Interfaces 2017, 9, 14808−14816

a few aggregates with a diameter of several tenths of a nanometer first appear in the 4-h-aged film of PTB7-Th/$PC_{61}BM$. Both the number and size of these particles increase with heating time, forming submicrometer-sized clusters after 15 h of thermal treatment. As expected, Figure 5b indicates only a few aggregates are noticed in the long-term-aged PTB7-Th/$PC_{61}BM$:bis-$PC_{61}BM$ (8 wt %) film. Very interestingly, although this finding is similar to that reported for the P3HT/$PC_{61}BM$ and P3HT/$PC_{61}BM$:bis-$PC_{61}BM$ systems, the size of thermally induced clusters in the PTB7-Th/$PC_{61}BM$ is approximately 1 order of magnitude smaller than that of those in the P3HT/$PC_{61}BM$ blend.

Carrier mobility is well-known to affect importantly the photovoltaic behavior of polymer solar cells. To better understand how the change in thermally induced morphology influences cell performance, the electron and hole mobilities of the photoactive composite layers, which were aged at 100 °C for various periods, were determined by the space-charge-limited current (SCLC) method using an electron-only (ITO/SAM of 4-aminobenzoic acid/PTB7-Th:$PC_{61}BM$:bis-$PC_{61}BM$ (without and with 8 wt %)/Ca/Al) and a hole-only (ITO/PEDOT:PSS/PTB7-Th:$PC_{61}BM$:bis-$PC_{61}BM$ (without and with 8 wt %)/Au) diode device, respectively. By the Mott–Gurney law,[38] the SCLC current density in the diode is given by

$$J = (9/8)\varepsilon_0\varepsilon_r\mu(V_{in}^2/d^3) \quad (1)$$

where ε_0 denotes the permittivity of a vacuum; ε_r is the relative dielectric constant of the sample; μ represents the charge carrier mobility; d is the thickness of the sample; and V_{in} is the voltage drop across the sample, which can be estimated from the equation $V_{in} = V_{app} - V_{bi}$, where V_{app} is the applied voltage and V_{bi} is the built-in voltage. Figures S2 and S3 plot the J–V curves as ln J versus ln V_{in} and, therefore, the carrier mobility can be determined from the intercept among fitting lines. Table 2 lists the obtained values. For the PTB7-Th/$PC_{61}BM$ diode, as

Table 2. Electron and Hole Mobility of PTB7-Th/$PC_{61}BM$:bis-$PC_{61}BM$ (without and with 8 wt %) Films with Long-Term Thermal Annealing at 100 °C, Determined by the SCLC Method

bis-$PC_{61}BM$ (wt %)	annealing time (min)	μ_e ($cm^2\ V^{-1}\ s^{-1}$)	μ_h ($cm^2\ V^{-1}\ s^{-1}$)	μ_e/μ_h
0	0	5.44×10^{-4}	1.45×10^{-4}	3.75
	60	4.37×10^{-4}	1.29×10^{-4}	3.39
	240	4.12×10^{-4}	8.54×10^{-5}	4.82
	480	3.55×10^{-4}	6.75×10^{-5}	5.26
	900	2.75×10^{-4}	1.26×10^{-5}	21.83
8	0	3.59×10^{-4}	1.21×10^{-4}	2.97
	60	4.11×10^{-4}	1.20×10^{-4}	3.43
	240	3.50×10^{-4}	8.06×10^{-5}	4.34
	480	3.77×10^{-4}	6.29×10^{-5}	6.00
	900	3.57×10^{-4}	5.86×10^{-5}	6.09

thermal aging time increases, the electron mobility (μ_e) gradually decreases from 5.44×10^{-4} $cm^2\ V^{-1}\ s^{-1}$ for the as-cast sample to 2.75×10^{-4} $cm^2\ V^{-1}\ s^{-1}$ for the 15-h-annealed film, whereas the hole mobility (μ_h) declines at a faster rate from 1.45×10^{-4} to 1.26×10^{-5} $cm^2\ V^{-1}\ s^{-1}$, leading to extremely unbalanced charge carrier transport with a μ_e/μ_h ratio of ~22. Interestingly, this fact is completely at odds with the observation reported for the P3HT/$PC_{61}BM$ system, in which the decay rate of electron mobility is around 20 times faster than that of hole mobility,[21] suggesting the thermal stress has different impacts on the phase morphologies of the PTB7-Th/$PC_{61}BM$ and P3HT/$PC_{61}BM$ systems. In contrast, the PTB7-Th/$PC_{61}BM$:bis-$PC_{61}BM$ (8 wt %) film possesses sturdy charge transport. Upon aging at 100 °C for 15 h, its μ_e remains at a comparable value of $\sim 3.6 \times 10^{-4}$ $cm^2\ V^{-1}\ s^{-1}$ and the μ_h is reduced to about half of its original value. Evidently, utilizing bis-$PC_{61}BM$ as a coacceptor effectively improves the morphological stability of the PTB7-Th/$PC_{61}BM$ layer, counteracting external thermal activation.

Both GISAXS and GIWAXS techniques were used to gain insight into the structural evolution of pristine PTB7-Th, PTB7-Th/$PC_{61}BM$, and PTB7-Th/$PC_{61}BM$:bis-$PC_{61}BM$ (8 wt %) blend films during prolonged high-temperature treatment. The out-of-plane GIWAXS peak from the as-cast PTB7-Th film (Figure 6a) at scattering vector (Q_z) = 1.55 $Å^{-1}$ is from the (010) diffraction that corresponds to a π–π stacking distance of ~4 Å, indicating that the π–π stacking is perpendicular to the substrate. This dominant orientation is favorable to the transport of charge carriers to the electrodes in OPV devices. This result is consistent with the report in the literature.[5] Annealing the PTB7-Th films at 100 °C for 4 h shifts the position of the (010) peak to 1.6 $Å^{-1}$ and substantially increases peak intensity, implying that thermal motion induces the formation of ordered and densely packed polymer chains. For ease of comparison with the PTB7-Th, Figure 6a also shows the out-of-plane GIWAXS profiles of the as-cast PTB7-Th/$PC_{61}BM$ and PTB7-Th/$PC_{61}BM$:bis-$PC_{61}BM$ (8 wt %) composite films. Both scattering profiles include a broad and intense peak at ~1.37 $Å^{-1}$, which corresponds to $PC_{61}BM$ aggregates whose scattering contrast is higher than that of PTB7-Th owing to the high electron density of the former,[33] causing the originally weak peak of the polymer crystallites at 1.55 $Å^{-1}$ to become an unclear shoulder. In contrast to the crystal growth of pristine PTB7-Th upon thermal aging, Figure 6b shows that the GIWAXS profile of the PTB7-Th/$PC_{61}BM$ film remains almost unchanged from the as-cast to the 4-h-annealed state, probably because $PC_{61}BM$ aggregation and polymer crystallization are mutually inhibited in the blend film by the spatial confinement during the annealing. However, extending the annealing time to 15 h causes the growth of $PC_{61}BM$ aggregates, as revealed by the intensified peak at 1.37 $Å^{-1}$. On the other hand, Figure 6c indicates that the PTB7-Th/$PC_{61}BM$:bis-$PC_{61}BM$ (8 wt %) three-component blend has an extremely stable GIWAXS profile throughout 15 h of annealing at 100 °C, demonstrating that the film that contains bis-$PC_{61}BM$ exhibits excellent morphological stability against the thermal aggregation of $PC_{61}BM$ molecules within the PTB7-Th matrix.

The GISAXS profiles that are recorded along the in-plane direction (parallel to the film surface) provide valuable information that can be used to probe the BHJ structure in the inner film. For pristine PTB7-Th, as presented in Figure 7a, the up-turn intensity in the low-Q region of the GISAXS profiles increases rapidly with the annealing time, revealing that the high-temperature environment accelerates the growth of crystalline domains whose sizes become even larger than 200 nm, which is above the detection limit, corresponding to the lowest Q value, 0.003 $Å^{-1}$, of the instrument used. With respect to the as-cast composite films, the lack of a perceptible difference between the GISAXS profiles of the PTB7-Th/

DOI: 10.1021/acsami.7b01296
ACS Appl. Mater. Interfaces 2017, 9, 14808–14816

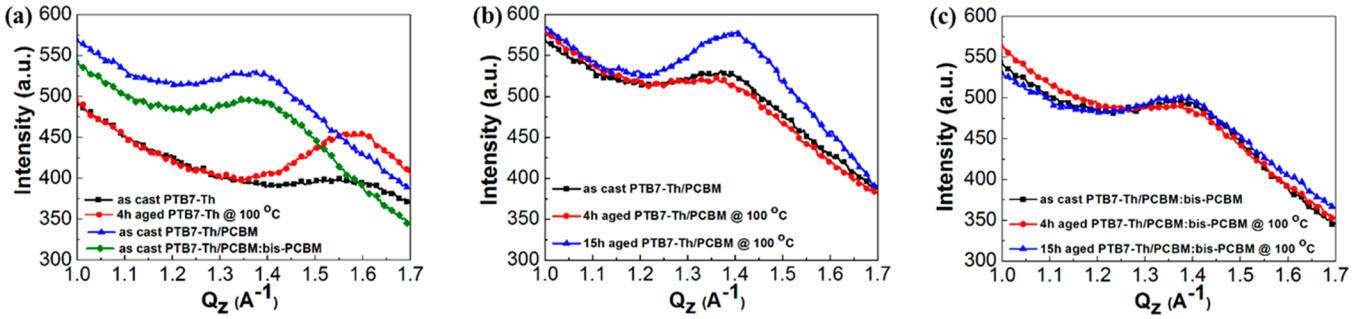

Figure 6. Temporal variation of the out-of-plane GIWAXS profiles for (a) pristine PTB7-Th, PTB7-Th/$PC_{61}BM$, and PTB7-Th/$PC_{61}BM$:bis-$PC_{61}BM$ (8 wt %) films, (b) as-cast and thermally aged PTB7-Th/$PC_{61}BM$ films, and (c) as-cast and thermally aged PTB7-Th/$PC_{61}BM$:bis-$PC_{61}BM$ (8 wt %) films.

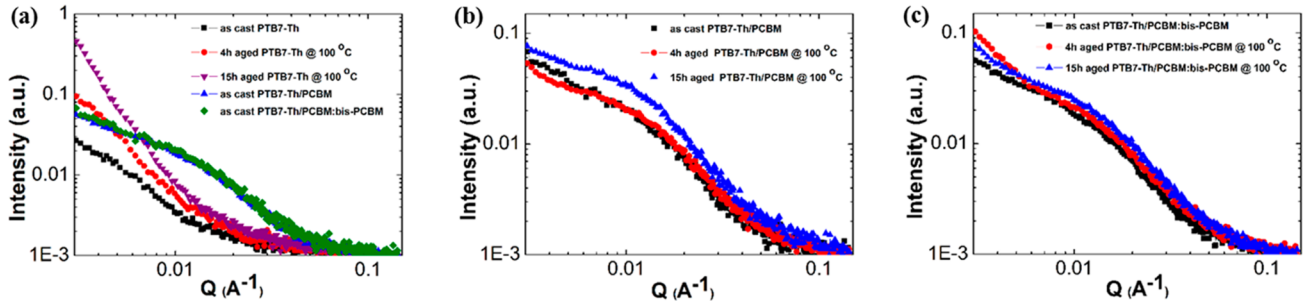

Figure 7. Temporal variation of the out-of-plane GISAXS profiles for (a) pristine PTB7-Th, PTB7-Th/$PC_{61}BM$, and PTB7-Th/$PC_{61}BM$:bis-$PC_{61}BM$ (8 wt %) films, (b) as-cast and thermally aged PTB7-Th/$PC_{61}BM$ films, and (c) as-cast and thermally aged PTB7-Th/$PC_{61}BM$:bis-$PC_{61}BM$ (8 wt %) films.

$PC_{61}BM$ with and without bis-$PC_{61}BM$ suggests that the partial replacement of $PC_{61}BM$ with bis-$PC_{61}BM$ has no significant influence on the phase morphology that is established during casting. According to the well-known rule $D = 2\pi/Q$, where D is the probe size and Q is the scattering vector, the shoulder at 0.016−0.02 $Å^{-1}$ of the GISAXS profiles of both composite films is indicative of pristine $PC_{61}BM$ aggregates with sizes of ∼30−40 nm. The GISAXS shoulder and the estimated size are consistent with those reported by other groups.[33,34] This size is about 1 order of magnitude greater than that of the $PC_{61}BM$ clusters (∼4 nm) in the as-cast P3HT/$PC_{61}BM$ blend film.[39] The relatively low crystallinity of PTB7-Th may be responsible for the generation of a few small polymer crystallites that consequently imposes less interference and steric hindrance on the growth of pristine $PC_{61}BM$ clusters. During the first 4 h of heating, the structure of pristine $PC_{61}BM$ nanodomains in the PTB7-Th/$PC_{61}BM$ remains stable, as evidenced by the unchanged GISAXS profiles in Figure 7b. However, Figure 2 shows that the PCE of the PTB7-Th/$PC_{61}BM$ cell drops by ∼20% and V_{oc}, J_{sc}, and FF are degraded after 4 h of thermal aging. This decay may be attributed to the formation of a few mesoscale $PC_{61}BM$-rich domains, as observed in the TEM images in Figure 5a. As mentioned earlier, the GISAXS technique is rather insensitive at submicrometer probe length scales, which are those of TEM observations. Prolonging the heating process significantly stimulates the creation of more pristine $PC_{61}BM$ nanoclusters, as evidenced by the development of a prominent shoulder in the GISAXS and an intensified peak in the GIWAXS profiles of the 15-h-aged PTB7-Th/$PC_{61}BM$ in Figures 7b and 6b, respectively. Interestingly, the size of these $PC_{61}BM$ clusters remains almost the same at ∼30−40 nm upon thermal annealing, implying that those submicrometer-sized clusters in the TEM images are not just random aggregations of pristine $PC_{61}BM$ clusters. Rather, these pristine $PC_{61}BM$ nanoclusters may induce the accumulation of $PC_{61}BM$ molecules and amorphous polymer chains by thermal diffusion to produce mesoscale $PC_{61}BM$-rich domains, which are the black dots in the TEM micrographs in Figure 5a. The scattering in the low-Q region of the GISAXS profile is contributed by the polymer crystallites and the macro-scale $PC_{61}BM$-rich domains. Although the scattering from the $PC_{61}BM$-rich aggregates becomes stronger after prolonged heating, the total scattering intensity at $Q \sim 0.003$ $Å^{-1}$ for a 15-h-aged film remains close to that of the as-cast film. This finding implies that ordered domains of polymer chains were partially deteriorated during long-term treatment at high temperature. The presence of $PC_{61}BM$ clusters and $PC_{61}BM$-rich domains may impede the percolation of polymer crystallites. Both effects contribute to the abrupt decline of hole mobility during annealing.

Conversely, the structure of pristine $PC_{61}BM$ nanoclusters within the PTB7-Th matrix for the film with 8 wt % bis-$PC_{61}BM$ is extremely robust against thermal stress, as supported by the stable GISAXS and GIWAXS profiles in Figures 7c and 6c, respectively, so the generation of submicrometer-sized $PC_{61}BM$-rich domains is effectively suppressed, as indicated by the TEM images in Figure 5b. Each bis-$PC_{61}BM$ molecule bears two bulky substituents, which may provide sufficient steric hindrance to prevent the generation of new $PC_{61}BM$ clusters by the $\pi-\pi$ interactions of fullerene cages and to obstruct the thermal accumulation of amorphous polymers and $PC_{61}BM$ molecules with nanoscale $PC_{61}BM$ clusters to form mesoscale $PC_{61}BM$-rich domains. From the mechanistic point of view, the mesoscale $PC_{61}BM$-rich domains would coalescence or connect the macroscale $PC_{61}BM$-rich segregations by the further accumulation of $PC_{61}BM$ molecules.

DOI: 10.1021/acsami.7b01296
ACS Appl. Mater. Interfaces 2017, 9, 14808−14816

The key parameter improving the thermal stability of these solar devices is the hindrance of thermal diffusion of $PC_{61}BM$ molecules and amorphous polymer segments toward the nanoscale clusters nearby to form a mesoscale $PC_{61}BM$-rich domain. The bis-$PC_{61}BM$ molecules have significant effect on the formations of nanoscale $PC_{61}BM$ clusters and mesoscale $PC_{61}BM$-rich domains.

CONCLUSION

The phase domains in the blend of $PC_{61}BM$ and PTB7-Th, a widely studied LBG polymer, are unstable in an elevated-temperature environment, causing a significant loss of the PCE of PTB7-Th/$PC_{61}BM$ BHJ solar cells, severely limiting their practical use. In the spin-drying process, portions of $PC_{61}BM$ molecules gather into several clusters with sizes of tens of nanometers that simultaneously restrict the growth of PTB7-Th crystallites by spatial confinement. In the early stage of annealing at 100 °C, these $PC_{61}BM$ clusters may promote the generation of $PC_{61}BM$-rich domains with submicrometer sizes. Prolonged thermal aging increases the population of $PC_{61}BM$ aggregates as well as the $PC_{61}BM$-rich clusters. The pristine $PC_{61}BM$ aggregates in the PTB7-Th/$PC_{61}BM$ are about 10 times larger than those in the P3HT/$PC_{61}BM$ film, so they may impose a greater spatial restriction on the development of large ordered domains of PTB7-Th. Moreover, clusters of both types may break the continuous pathways along which holes are transported to the anode. This suggestion is evidenced by the rapid drop of hole mobility in the course of high-temperature treatment. Although the substitution of a small amount of $PC_{61}BM$ with bis-$PC_{61}BM$ only slightly alters the size of fullerene clusters, it not only prevents the generation of additional fullerene aggregates but also almost completely prevents the creation of submicrometer-sized $PC_{61}BM$-rich clusters under thermal stress, leading to an extremely stable morphology. This is probably because the two bulky and randomly distributed organic moieties on bis-$PC_{61}BM$ sterically obstruct the formation of the aforementioned clusters via the dense packing of C_{60} cages. Consequently, the application of this three-component blend as an active layer markedly reduces the PCE drop from ∼60% for that without bis-$PC_{61}BM$ to <10% following isothermal aging for 15 h. This investigation provides insights into the morphological evolution of LBG polymer-based active layers from nanoscale to microscale domains at an elevated temperature of 100 °C, which simulates harsh operational conditions. Additionally, this work demonstrates a simple but effective approach to substantially reducing the decay of cell performance that arises from morphological degradation by thermal stress.

EXPERIMENTAL METHODS

Materials. The LBG conjugated polymer (PTB7-Th) and poly(3,4-ethylenedioxythiophene):poly(styrenesulfonate) (PEDOT:PSS) (CLEVIOS P VP AI 4083) were purchased from 1-Material Inc. and Heraeus Precious Metals GmbH & Co. KG, respectively. $PC_{61}BM$ (99%) and bis-$PC_{61}BM$ (>99.5%) were supplied by Nano-C Inc. Other chemical reagents were purchased from ACROS and directly used without further purification.

Instruments and Characterization. All current−voltage (J−V) curves of PSCs were measured using a Keithley 2400 source instrument with a scan rate of 0.1 V s^{-1} (from −0.5 to 1.0 V) at ambient condition (20 °C, in air) under Air Mass 1.5 Global (AM 1.5 G) illumination, which was provided by a 300 W solar simulator (Oriel 91160), at an intensity of 100 mW cm^{-2}. A 300 W solar simulator (Oriel 91160) was used as the light source for J−V measurements, and the light intensity was calibrated using a monocrystalline silicon reference cell with a KG-5 filter (PV Measurements, Inc.), which was precalibrated by the National Renewable Energy Laboratory (NREL). The spectral mismatch factor in our measurement system was determined from the spectral data of the device, the reference cell, and the solar simulator following the procedure reported in the VLSI standards document 0245161-000 and found to be 0.9968. The IPCE spectra were measured using a xenon lamp with a monochromator (Triax 180, Jobin Yvon) as the light source, and the light intensity was calibrated by an Ophir 2A-SH thermopile detector. OM images were captured by a Sony (EXWAVE HAD CCD sensor) microscope. TEM images were obtained from a Hitachi H-7100 microscope. The measurements of the simultaneous GISAXS and GIWAXS were performed using the BL23A beamline of the National Synchrotron Radiation Center (NSRRC) in Taoyuan, Taiwan. The film thickness was determined by a stylus profiler (α-Step DETAK 6m, Digital Instruments, Inc./Veeco Metrology Group).

Fabrication of BHJ PSCs. All BHJ PSCs were fabricated with a regular sandwich structure, ITO/PEDOT:PSS/PTB7-Th:$PC_{61}BM$:bis-$PC_{61}BM$ (without or with 2, 4, and 8 wt %)/Ca/Al. The ITO glasses were cleaned in detergent (5 min), deionized water (5 min), acetone (10 min), and then isopropanol (10 min) using an ultrasonic oscillator, followed by drying these substrates under a nitrogen stream for 10 s. The PEDOT:PSS suspension was filtered through a 0.2 μm filter and then spin-coated on top of cleaned ITO glasses at a spin rate of 3500 rpm for 30 s to form a hole transport layer with a thickness of ∼30 nm. After being baked on a hot plate at 140 °C for 10 min, the substrates were delivered into a glovebox having O_2 and H_2O contents of <0.1 ppm and spin-coated (800 rpm, 30 s) with a coating solution comprising PTB7-Th (10.0 mg), $PC_{61}BM$ (15.0 mg), and chlorobenzene (1.0 mL), which were mixed by magnetic stirring at 50 °C for 24 h, to generate the active layers with a thickness of ∼100 nm. For preparing the PTB7-Th:$PC_{61}BM$:bis-$PC_{61}BM$ three-component films, various amounts (0.3, 0.6, or 1.2 mg) of $PC_{61}BM$ were replaced with bis-$PC_{61}BM$. These composite films were then thermally aged at 100 °C for various periods to study the thermal stability of morphology. Finally, layers of calcium (∼20 nm) and aluminum (∼60 nm) were subsequently deposited on top of the active layer as metal electrode by a homemade thermal evaporator (3×10^{-5} Pa) to finish device fabrication. The active area of all devices is 0.06 cm^2.

Preparation of GIWAXS/GISAXS Samples. The multilength-scale morphology of PTB7-Th and $PC_{61}BM$ blends was examined using the GIWAXS/GISAXS instrument. A 100 nm active layer of pristine PTB7-Th, PTB7-Th/$PC_{61}BM$, or PTB7-Th/$PC_{61}BM$:bis-$PC_{61}BM$ (8 wt %) was spin coated onto a cleaned Si wafer substrate (1×1 cm^2) at 800 rpm for 30 s under a nitrogen atmosphere. These thin films were dried in vacuum for 20 min and subsequently thermally heated at 100 °C for 0 (as cast), 240, or 900 min in a nitrogen-filled glovebox. The simultaneous GISAXS/GIWAXS measurements were performed at the BL-23 beamline of NSRRC. The instrumental configuration and experiment procedure were described elsewhere.[37,40] In the GISAXS/GIWAXS measurements, the incident angle to each thin film was aligned precisely to 0.2 ± 0.002°. The 2D GIWAXS patterns of the pristine PTB7-Th and PTB7-Th/$PC_{61}BM$ blend films shows that the diffraction spots dominate in the out-of-plane direction (i.e., perpendicular to the film or substrate surface), indicating the preferred orientation of polymer crystallites. Thus, the main 1D GIWAXS profiles were reduced from the out-of-plane direction and expressed as a function of scattering vector Q_z. The 1D profile GISAXS profiles were mainly reduced from the in-plane direction (parallel to the film surface) by a horizontal cut covering the Yoneda peak and expressed as a function of scattering vector Q_x for solving the BHJ film structure.[39,41] Previous studies showed the effect of the active layers coated on the PEDOT:PSS/Si and pure Si substrates on the GISAXS/GIWAXS intensities can be negligible.[40,42]

DOI: 10.1021/acsami.7b01296
ACS Appl. Mater. Interfaces 2017, 9, 14808−14816

■ ASSOCIATED CONTENT

Supporting Information

The Supporting Information is available free of charge on the ACS Publications website at DOI: 10.1021/acsami.7b01296.

J−*V* curves of as-cast PTB7-Th/$PC_{61}BM$:bis-$PC_{61}BM$ (without or with 2, 4, and 8 wt %) solar devices; PCE statistic plots and photovoltaic parameters of as-cast and thermally aged PTB7-Th/$PC_{61}BM$ and PTB7-Th/$PC_{61}BM$:bis-$PC_{61}BM$ solar cells; space-charge-limited *J*−*V* curves of electron-only and hole-only devices based on PTB7-Th/$PC_{61}BM$ and PTB7-Th/$PC_{61}BM$:bis-$PC_{61}BM$ (8 wt %) active layer, which were annealed at 100 °C for various periods of time (PDF)

■ AUTHOR INFORMATION

Corresponding Authors

*(C.-S.T.) E-mail: cstsao@iner.gov.tw.

*(L.W.) Phone: +886-2-3366-5276. Fax: +886-2-2365-5404. E-mail: leewang@ntu.edu.tw.

ORCID

Leeyih Wang: 0000-0002-6368-0141

Notes

The authors declare no competing financial interest.

■ ACKNOWLEDGMENTS

We thank the Ministry of Science and Technology, Republic of China (102-2113-M-002-003-MY3; 104-2911-I-002−574; 105-3113-E-002-010), and Academia Sinica, Taiwan (AS-103-SS-A02), for financially supporting this research.

■ REFERENCES

(1) Cui, C.; He, Z.; Wu, Y.; Cheng, X.; Wu, H.; Li, Y.; Cao, Y.; Wong, W. Y. High-Performance Polymer Solar Cells Based on a 2D-Conjugated Polymer with an Alkylthio Side-Chain. *Energy Environ. Sci.* **2016**, *9*, 885−891.

(2) Kuo, C. Y.; Nie, W.; Tsai, H.; Yen, H. J.; Mohite, A. D.; Gupta, G.; Dattelbaum, A. M.; William, D. J.; Cha, K. C.; Yang, Y.; Wang, L.; Wang, H. L. Structural Design of Benzo[1,2-b:4,5-b′]dithiophene-Based 2D Conjugated Polymers with Bithienyl and Terthienyl Substituents Toward Photovoltaic Applications. *Macromolecules* **2014**, *47*, 1008−1020.

(3) Nikiforov, M. P.; Lai, B.; Chen, W.; Chen, S.; Schaller, R. D.; Strzalka, J.; Maser, J.; Darling, S. B. Detection and Role of Trace Impurities in High-Performance Organic Solar Cells. *Energy Environ. Sci.* **2013**, *6*, 1513−1520.

(4) Li, N.; Brabec, C. J. Air-Processed Polymer Tandem Solar Cells with Power Conversion Efficiency Exceeding 10%. *Energy Environ. Sci.* **2015**, *8*, 2902−2909.

(5) Lu, L.; Yu, L. Understanding Low Bandgap Polymer PTB7 and Optimizing Polymer Solar Cells Based on It. *Adv. Mater.* **2014**, *26*, 4413−4430.

(6) Liang, Y.; Xu, Z.; Xia, J.; Tsai, S. T.; Wu, Y.; Li, G.; Ray, C.; Yu, L. For the Bright Future—Bulk Heterojunction Polymer Solar Cells with Power Conversion Efficiency of 7.4%. *Adv. Mater.* **2010**, *22*, E135−E138.

(7) He, Z.; Zhong, C.; Su, S.; Xu, M.; Wu, H.; Cao, Y. Enhanced Power-Conversion Efficiency in Polymer Solar Cells Using an Inverted Device Structure. *Nat. Photonics* **2012**, *6*, 591−595.

(8) Liao, S. H.; Jhuo, H. J.; Cheng, Y. S.; Chen, S. A. Fullerene Derivative-Doped Zinc Oxide Nanofilm as the Cathode of Inverted Polymer Solar Cells with Low-Bandgap Polymer (PTB7-Th) for High Performance. *Adv. Mater.* **2013**, *25*, 4766−4771.

(9) Liao, S. H.; Jhuo, H. J.; Yeh, P. N.; Cheng, Y. S.; Li, Y. L.; Lee, Y. H.; Sharma, S.; Chen, S. A. Single Junction Inverted Polymer Solar Cell Reaching Power Conversion Efficiency 10.31% by Employing Dual-Doped Zinc Oxide Nano-Film as Cathode Interlayer. *Sci. Rep.* **2014**, *4*, 6813−6819.

(10) Cheng, Y. J.; Yang, S. H.; Hsu, C. S. Synthesis of Conjugated Polymers for Organic Solar Cell Applications. *Chem. Rev.* **2009**, *109*, 5868−5923.

(11) Chen, W.; Nikiforov, M. P.; Darling, S. B. Morphology Characterization in Organic and Hybrid Solar Cells. *Energy Environ. Sci.* **2012**, *5*, 8045−8074.

(12) Nguyen, T. P.; Girault, P.; Renaud, C.; Reisdorffer, F.; Le Rendu, P.; Wang, L. Effects of the Negative Electrode Contact on the Performance of Poly(hexylthiophene):6,6-phenyl-C_{61}-butyric Acid Methyl Ester Based Organic Solar Cells. *J. Appl. Phys.* **2014**, *115*, 012013−012019.

(13) Dang, M. T.; Hirsch, L.; Wantz, G.; Wuest, J. D. Controlling the Morphology and Performance of Bulk Heterojunctions in Solar Cells. Lessons Learned from the Benchmark Poly(3-hexylthiophene):[6,6]-Phenyl-C_{61}-butyric Acid Methyl Ester System. *Chem. Rev.* **2013**, *113*, 3734−3765.

(14) Huang, Y.; Kramer, E. J.; Heeger, A. J.; Bazan, G. C. Bulk Heterojunction Solar Cells: Morphology and Performance Relationships. *Chem. Rev.* **2014**, *114*, 7006−7043.

(15) Nguyen, L. H.; Hoppe, H.; Erb, T.; Günes, S.; Gobsch, G.; Sariciftci, N. S. Effects of Annealing on the Nanomorphology and Performance of Poly(alkylthiophene):Fullerene Bulk-Heterojunction Solar Cells. *Adv. Funct. Mater.* **2007**, *17*, 1071−1078.

(16) Li, G.; Yao, Y.; Yang, H.; Shrotriya, V.; Yang, G.; Yan, Y. "Solvent Annealing" Effect in Polymer Solar Cells Based on Poly(3-hexylthiophene) and Methanofullerenes. *Adv. Funct. Mater.* **2007**, *17*, 1636−1644.

(17) Ma, W.; Yang, C.; Gong, X.; Lee, K.; Heeger, A. J. Thermally Stable, Efficient Polymer Solar Cells with Nanoscale. Control of the Interpenetrating Network Morphology. *Adv. Funct. Mater.* **2005**, *15*, 1617−1622.

(18) Yao, Y.; Hou, J.; Xu, Z.; Li, G.; Yang, Y. Effects of Solvent Mixtures on the Nanoscale Phase Separation in Polymer Solar Cells. *Adv. Funct. Mater.* **2008**, *18*, 1783−1789.

(19) Chang, Y.-M.; Wang, L. Efficient Poly(3-hexylthiophene)-Based Bulk Heterojunction Solar Cells Fabricated by an Annealing-Free Approach. *J. Phys. Chem. C* **2008**, *112*, 17716−17720.

(20) Steiner, M. A.; Geisz, J. F.; Friedman, D. J.; Olavarria, W. J.; Duda, A.; Moriarty, T. E. *Proceedings of 37th IEEE Photovoltaic Specialists Conference*, Seattle, WA, USA, June 19−24, 2011.

(21) Liu, H. W.; Chang, D. Y.; Chiu, W. Y.; Rwei, S. P.; Wang, L. Fullerene Bisadduct As an Effective Phase-Separation Inhibitor in Preparing Poly(3-hexylthiophene)-[6,6]-phenyl-C_{61}-butyric Acid Methyl Ester Blends with Highly Stable Morphology. *J. Mater. Chem.* **2012**, *22*, 15586−15591.

(22) Sivula, K.; Luscombe, C. K.; Thompson, B. C.; Fréchet, J. M. J. Enhancing the Thermal Stability of Polythiophene:Fullerene Solar Cells by Decreasing Effective Polymer Regioregularity. *J. Am. Chem. Soc.* **2006**, *128*, 13988−13989.

(23) Bertho, S.; Janssen, G.; Cleij, T. J.; Conings, B.; Moons, W.; Gadisa, A.; D'Haen, J.; Goovaerts, E.; Lutsen, L.; Manca, J.; Vanderzande, D. Effect of Temperature on the Morphological and Photovoltaic Stability of Bulk Heterojunction Polymer:Fullerene Solar Cells. *Sol. Energy Mater. Sol. Cells* **2008**, *92*, 753−760.

(24) Sivula, K.; Ball, Z. T.; Watanabe, N.; Frechet, J. M. J. Amphiphilic Diblock Copolymer Compatibilizers and Their Effect on the Morphology and Performance of Polythiophene:Fullerene Solar Cells. *Adv. Mater.* **2006**, *18*, 206−210.

(25) Lee, Y. H.; Chen, W. C.; Chiang, C. J.; Kau, K. C.; Liou, W. S.; Lee, Y. P.; Wang, L.; Dai, C. A. A New Strategy for Fabricating Organic Photovoltaic Devices with Stable D/A Double-Channel Network to Enhance Performance Using Self-Assembling All-Conjugated Diblock Copolymer. *Nano Energy* **2015**, *13*, 103−116.

(26) Hsieh, C. H.; Cheng, Y. J.; Li, P. J.; Chen, C. H.; Dubosc, M.; Liang, R. M.; Hsu, C. S. Highly Efficient and Stable Inverted Polymer

Solar Cells Integrated with a Cross-Linked Fullerene Material as an Interlayer. *J. Am. Chem. Soc.* **2010**, *132*, 4887−4893.
(27) Zhang, Y.; Yip, H. L.; Acton, O.; Hau, S. K.; Huang, F.; Jen, A. K. Y. A Simple and Effective Way of Achieving Highly Efficient and Thermally Stable Bulk-Heterojunction Polymer Solar Cells Using Amorphous Fullerene Derivatives as Electron Acceptor. *Chem. Mater.* **2009**, *21*, 2598−2600.
(28) Azimi, H.; Senes, A.; Scharber, M. C.; Hingerl, K.; Brabec, C. J. Charge Transport and Recombination in Low-Bandgap Bulk Heterojunction Solar Cell using Bis-adduct Fullerene. *Adv. Energy Mater.* **2011**, *1*, 1162−1168.
(29) Miller, N. C.; Sweetnam, S.; Hoke, E. T.; Gysel, R.; Miller, C. E.; Bartelt, J. A.; Xie, X.; Toney, M. F.; McGehee, M. D. Molecular Packing and Solar Cell Performance in Blends of Polymers with a Bisadduct Fullerene. *Nano Lett.* **2012**, *12*, 1566−1570.
(30) Raja, R.; Liu, W. S.; Hsiow, C. Y.; Hsieh, Y. J.; Rwei, S. P.; Chiu, W. Y.; Wang, L. Novel Fulleropyrrolidines Bearing-Conjugated Thiophene Derivatives as Compatibilizing Group for Developing Highly Stable Polymer Solar Cells. *Org. Electron.* **2014**, *15*, 2223−2233.
(31) Saravanan, C.; Liu, C. L.; Chang, Y. M.; Lu, J. D.; Hsieh, Y. J.; Rwei, S. P.; Wang, L. [60]Fulleropyrrolidines Bearing π-Conjugated Moiety for Polymer Solar Cells: Contribution of the Chromophoric Substituent on C_{60} to the Photocurrent. *ACS Appl. Mater. Interfaces* **2012**, *4*, 6133−6141.
(32) Chen, Y. H.; Huang, P. T.; Lin, K. C.; Huang, Y. J.; Chen, C. T. Stabilization of Poly(3-hexylthiophene)/PCBM Morphology by Hydroxyl Group End-Functionalized P3HT and Its Application to Polymer Solar Cells. *Org. Electron.* **2012**, *13*, 283−289.
(33) Chen, W.; Xu, T.; He, F.; Wang, W.; Wang, C.; Strzalka, J.; Liu, Y.; Wen, J.; Miller, D. J.; Chen, J.; Hong, K.; Yu, L.; Darling, S. B. Hierarchical Nanomorphologies Promote Exciton Dissociation in Polymer/Fullerene Bulk Heterojunction Solar Cells. *Nano Lett.* **2011**, *11*, 3707−3713.
(34) Liu, F.; Zhao, W.; Tumbleston, J. R.; Wang, C.; Gu, Y.; Wang, D.; Briseno, A. L.; Ade, H.; Russell, T. P. Understanding the Morphology of PTB7:PCBM Blends in Organic Photovoltaics. *Adv. Energy Mater.* **2014**, *4*, 1301377−1301385.
(35) Guo, S.; Herzig, E. M.; Naumann, A.; Tainter, G.; Perlich, J.; Müller-Buschbaum, P. Influence of Solvent and Solvent Additive on the Morphology of PTB7 Films Probed via X-ray Scattering. *J. Phys. Chem. B* **2014**, *118*, 344−350.
(36) Collins, B. A.; Li, Z.; Tumbleston, J. R.; Gann, E.; McNeill, C. R.; Ade, H. Absolute Measurement of Domain Composition and Nanoscale Size Distribution Explains Performance in PTB7:PC71BM Solar Cells. *Adv. Energy. Mater.* **2013**, *3*, 65−74.
(37) Liao, H. C.; Tsao, C. S.; Lin, T. H.; Jao, M. H.; Chuang, C. M.; Chang, S. Y.; Huang, Y. C.; Shao, Y. T.; Chen, C.-Y.; Su, C.-J.; Jeng, U. S.; Chen, Y. F.; Su, W. F. Nanoparticle-Tuned Self-Organization of a Bulk Heterojunction Hybrid Solar Cell with Enhanced Performance. *ACS Nano* **2012**, *6*, 1657−1666.
(38) Mott, N. F.; Gurney, R. W. *Electronic Processes in Ionic Crystals*, 1st ed.; Oxford University Press: New York, 1940.
(39) Chen, C. Y.; Tsao, C. S.; Huang, Y.-C.; Liu, H. W.; Chiu, W. Y.; Chuang, C. M.; Jeng, U. S.; Su, C. J.; Wu, W. R.; Su, W. F.; Wang, L. Mechanism and Control of the Structural Evolution of a Polymer Solar Cell from a Bulk Heterojunction to a Thermally Unstable Hierarchical Structure. *Nanoscale* **2013**, *5*, 7629−7638.
(40) Huang, Y. C.; Tsao, C. S.; Chuang, C. M.; Lee, C. H.; Hsu, F. H.; Cha, H. C.; Chen, C. Y.; Lin, T. H.; Su, C. J.; Jeng, U. S.; Su, W. F. Small- and Wide-Angle X-ray Scattering Characterization of Bulk Heterojunction Polymer Solar Cells with Different Fullerene Derivatives. *J. Phys. Chem. C* **2012**, *116*, 10238−10244.
(41) Andersen, T. R.; Larsen-Olsen, T. T.; Andreasen, B.; Bottiger, A. P. L.; Carle, J. E.; Helgesen, M.; Bundgaard, E.; Norrman, K.; Andreasen, J. W.; Jørgensen, M.; Krebs, F. C. Aqueous Processing of Low-Band-Gap Polymer Solar Cells Using Roll-to-Roll Methods. *ACS Nano* **2011**, *5*, 4188−4196.
(42) Liao, H. C.; Tsao, C. S.; Shao, Y. T.; Chang, S. Y.; Huang, Y. C.; Chuang, C. M.; Lin, T. H.; Chen, C. Y.; Su, C. J.; Jeng, U. S.; Chen, Y. F.; Su, W. F. Bi-Hierarchical Nanostructures of Donor−Acceptor Copolymer and Fullerene for High Efficient Bulk Heterojunction Solar Cells. *Energy Environ. Sci.* **2013**, *6*, 1938−1948.

DOI: 10.1021/acsami.7b01296
ACS Appl. Mater. Interfaces 2017, 9, 14808−14816